

Gear Mathematics for Bevel & Hypoid Gears

Hermann J. Stadtfeld

Bevel Gear Technology

Chapter 2

This article is the third installment in *Gear Technology's* series of excerpts from Dr. Hermann J. Stadtfeld's book, *Gleason Bevel Gear Technology*. The first two excerpts can be found in our June 2015 and July 2015 issues.

The goal of the following sections is to develop a deeper understanding of the function, limits and possibly the not fully utilized possibilities of bevel and hypoid gears.

The gear mathematics developed by the author is based on a triangular vector model that presents a comprehensive tool for simple observations in the generating gear, up to complex three-dimensional developments. Many types of bevel and hypoid gears can be observed and manipulated with this model — without alteration of the notation. However, at the most complex level the lengths and directions of the vectors change according to higher-order functions, depending on the rotational position of the generating gear (Refs. 1–2).

The first chapter of this book — “Nomenclature and Definition of Symbols” — should help to avoid or minimize the interruption of the flow in the gear theoretical developments with definitions of formula symbols.

At the beginning of this chapter the development of a face-milled, conjugate spiral bevel gearset is conducted. Next, an analogue face-hobbed bevel gearset is derived that in a third step is converted to a non-generated (Formate) version. In step four an offset is added to the Formate spiral bevel gearset that results in a hypoid gearset. Consequences regarding the introduction of the hypoid offset and unique facts regarding general spatial transmissions are also discussed in this chapter. At the end of this chapter, length and profile crowning are added to the Formate bevel gearset that delivers a practical-use, angular transmission as it is used in industrial gear boxes; the reader will be able to apply the derivations to any other bevel and hypoid gearset. With the results of each calculation step, basic settings are computed as they are commonly used by modern CNC bevel gear generators in order to cut or grind real bevel gearsets. —**Hermann J. Stadtfeld**

Development of a Face-Milled Spiral Bevel Gearset

The following data are given for this example:

Method	single indexing with Gleason straddle cut	
Tooth depth along face width	parallel	
Shaft angle	Σ	= 90°
Offset	$a = TTX$	= 0 mm
Number of pinion teeth	z_1	= 13
Number of ring gear teeth	z_2	= 35
Outer ring gear pitch diameter	D_{o2}	= 190 mm
Face width	$b_1 = b_2$	= 30 mm
Mean spiral angle	$\beta_1 = \beta_2$	= 30°
Pinion hand of spiral	$HOSP_1$	= left-hand
Nominal cutter radius	R_w	= 76.2 mm (6")
Pressure angle	$\alpha_c = \alpha_D$	= 20°
Profile shift factor	$x = x_1 = -x_2$	= 0
Tooth depth factor	f_{Depth}	= 1
Top-root-clearance factor	f_{CL}	= 0.2
Profile side shift factor	$x_S = x_{S1} = -x_{S2}$	= 0
Pinion addendum	$h_{K1} = (f_{Depth} + x) \times m_n$	= 1.0 m_n
Pinion dedendum	$h_{F1} = (f_{Depth} + f_{CL} - x) \times m_n$	= 1.2 m_n
Ring gear addendum	$h_{K2} = (f_{Depth} - x) \times m_n$	= 1.0 m_n
Ring gear dedendum	$h_{F2} = (f_{Depth} + f_{CL} + x) \times m_n$	= 1.2 m_n

Wanted are the design data of the pinion and ring gear blanks, as well as the cutter specifications and basic machine settings.

Calculation of Blank Data

The calculation begins with the computation of the ring gear blank data. The geometrically relevant parameters are shown in Figure 1. The position of the teeth relative to the blank coordinate system of a bevel gear blank is satisfactorily defined with

the following data: $RAUR$; $RINR$; γ ; $ZFKR$; $ZTKR$; and $ZKKR$. Those blank data are calculated from the given data as follows: (1)

$$z_1 / z_2 = \sin \gamma_1 / \sin \gamma_2$$

(Regarding Eq. 1, see also Eq.s 10–12, Chapter 1)

The sum of the pitch angles of spiral bevel gears is equal to the shaft angle:

$$\gamma_1 + \gamma_2 = \Sigma \rightarrow \gamma_1 = \Sigma - \gamma_2$$

In case of a 90° shaft angle the relationship will simplify to:

$$\gamma_1 = \arctan(z_1 / z_2) = 20.38 \quad (2)$$

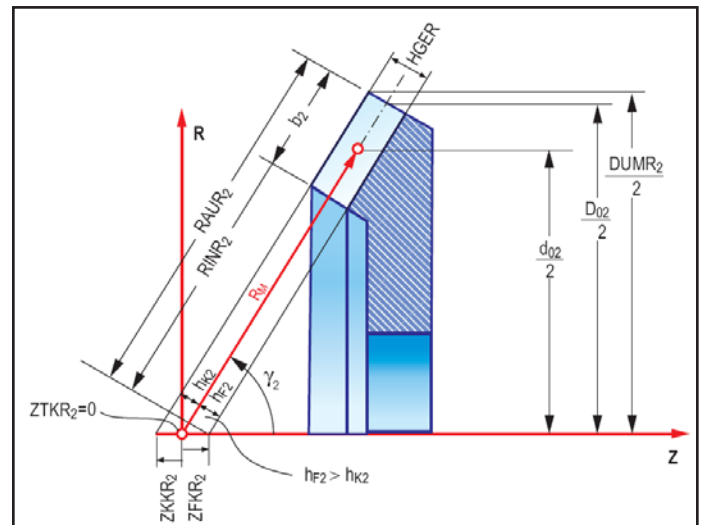


Figure 1 Graphical specification of ring gear blank.

$$\gamma_2 = 90^\circ - \gamma_1 = 69.62^\circ \quad (3)$$

Now the different cone distances, normal module, and mean pitch diameter can be calculated:

$$R_M = D_{02} / 2 / \sin \gamma_2 - b_2 / 2 = 86.34 \text{ mm} \quad (4)$$

$$d_{02} = 2 \times R_M \times \sin \gamma_2 = 161.87 \text{ mm} \quad (5)$$

$$m_f = d_{02} / z_2 = 4.63 \text{ mm} \quad (6)$$

$$m_n = m_f \times \cos \beta_2 = 4.00 \text{ mm} \quad (7)$$

$$h_{k2} = 1.0 \times m_n = 4.00 \text{ mm} \quad (8)$$

$$h_{f2} = 1.2 \times m_n = 4.80 \text{ mm} \quad (9)$$

$$RINR_2 = R_M - b_2 / 2 - h_{f2} / \tan \gamma_2 = 69.56 \text{ mm} \quad (10)$$

$$RAUR_2 = RINR_2 + b_2 = 99.56 \text{ mm} \quad (11)$$

The positions of the cone apexes, the whole depth and the maximal ring gear diameter are:

$$ZFKR_2 = +h_{f2} / \sin \gamma_2 = 5.12 \text{ mm} \quad (12)$$

$$ZKKR_2 = -h_{k2} / \sin \gamma_2 = -4.27 \text{ mm} \quad (13)$$

$$ZTKR_2 = 0.00 \text{ mm} \quad (14)$$

$$HGER = h_{k2} + h_{f2} = 8.80 \text{ mm} \quad (15)$$

$$DUMR_2 = 2(RAUR_2 \times \sin \gamma_2 + HGER \times \cos \gamma_2) = 192.78 \text{ mm} \quad (16)$$

Pinion pitch angle and mean cone distance R_M (which is equal for pinion and gear) have already been calculated in the course of the gear blank calculations. Only the inner and outer cone distance—as well as the cone apex positions—remain in the pinion blank calculation (Fig. 2). The value for addendum and dedendum is equal to the ring gear values, since no profile shift was applied to the present example:

$$h_{k1} = 1.0 \times m_n = 4.00 \text{ mm} \quad (17)$$

$$h_{f1} = 1.2 \times m_n = 4.80 \text{ mm} \quad (18)$$

$$RINR_1 = R_M - b_1 / 2 - h_{f1} / \tan \gamma_1 = 58.42 \text{ mm} \quad (19)$$

$$RAUR_1 = RINR_1 + b_1 = 88.42 \text{ mm} \quad (20)$$

The positions of the pinion cone apexes are:

$$ZFKR_1 = +h_{f1} / \sin \gamma_1 = 13.78 \text{ mm} \quad (21)$$

$$ZKKR_1 = -h_{k1} / \sin \gamma_1 = -11.49 \text{ mm} \quad (22)$$

$$ZTKR_1 = 0.00 \text{ mm} \quad (23)$$

All bold-printed parameters in this section are required for the definition of the toothed cones relative to the remaining pinion and gear blank. Those design data are summarized in Tables 1 and 2.

Calculation of Cutter Head Geometry

The nominal cutter radius was chosen a little bit smaller than the mean cone distance R_M . This seems to be a good choice for a face-milled (single indexing process) bevel gearset if large load-affected deformations are anticipated.

Although the nominal cutter radius is already given, the actual radii of inside and outside blades for gear and pinion cutter head have to be calculated depending on the chosen cut-

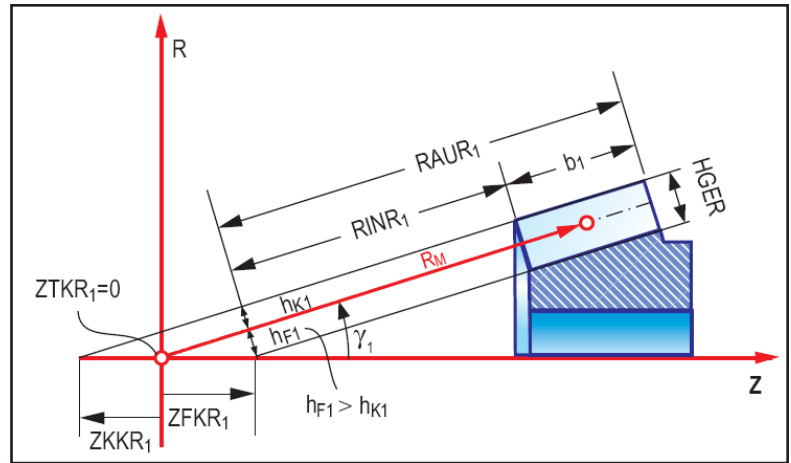


Figure 2 Pinion blank specification.

Table 1 Numerical ring gear blank specifications

Ring Gear - Blank Data			
Variable	Explanation	Value	Dimension
z_2	number of ring gear teeth	35	-
$RINR_2$	inner cone distance (along root line)	69.56	mm
$RAUR_2$	outer cone distance (along root line)	99.56	mm
$GATR_2 = \gamma_2$	pitch angle	69.62	°
$GAKR_2$	face angle	69.62	°
$GAFR_2$	root angle	69.62	°
$ZTKR_2$	pitch apex to crossing point	0.00	mm
$ZKKR_2$	face apex to crossing point	-4.27	mm
$ZFKR_2$	root apex to crossing point	5.12	mm
$DOMR_2 = m_f$	face module	4.63	mm
$HGER$	whole depth of teeth	8.80	mm

Table 2 Numerical pinion blank specifications

Pinion - Blank Data			
Variable	Explanation	Value	Dimension
z_1	number of teeth pinion	13	-
$RINR_1$	inner cone distance (along root line)	58.42	mm
$RAUR_1$	outer cone distance (along root line)	88.42	mm
$GATR_1 = \gamma_1$	pitch angle	20.38	°
$GAKR_1$	face angle	20.38	°
$GAFR_1$	root angle	20.38	°
$ZTKR_1$	pitch apex to crossing point	0.00	mm
$ZKKR_1$	face apex to crossing point	-11.49	mm
$ZFKR_1$	root apex to crossing point	13.78	mm
$DOMR_1 = m_f$	face module	4.63	mm
$HGER$	whole depth of teeth	8.80	mm

For Related Articles Search

bevel gears

at www.geartechnology.com

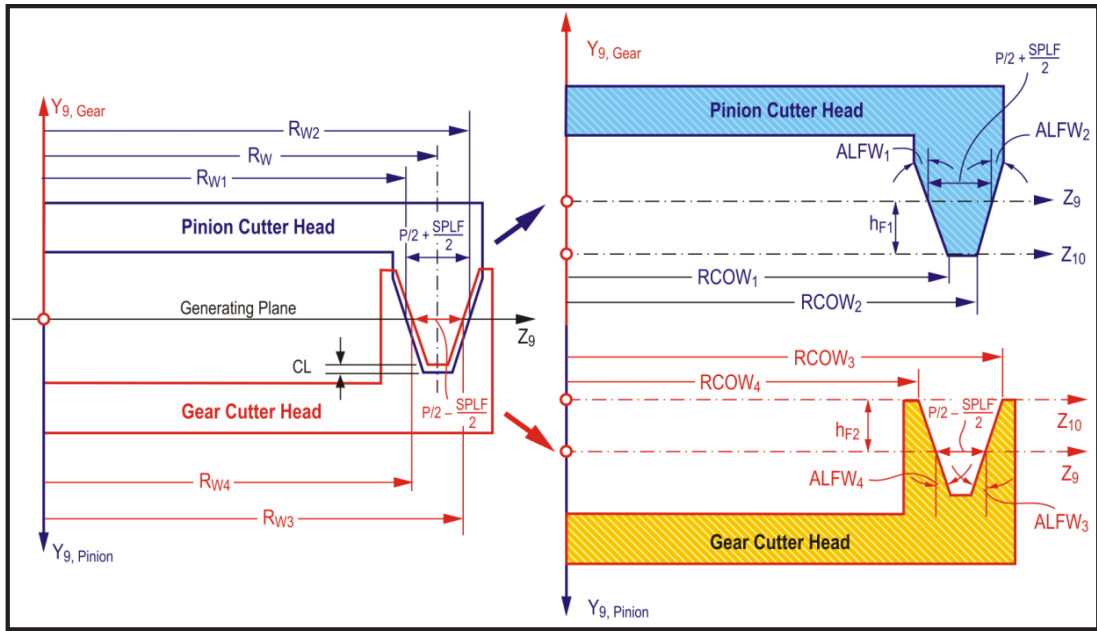


Figure 3 Pinion and ring gear blade geometry.

ting method. Since the method is Gleason straddle cut, the pinion blades cut a tooth slot while the gear blades are cutting a tooth — i.e., two proceeding “half-slots.”

Figure 3 shows (left) the corresponding blades of pinion and ring gear (see also Figs. 12–15, Chap. 1, Part II, July Gear Technology). The generating plane intersects with the blades at the height of the calculation point. In order to generate the correct tooth thickness, the distance from the calculation point on the inside blade to the calculation point on the outside blade has to be equal to one-half of the normal pitch, plus one-half of the normal backlash. The blade tips extend about the tooth dedendum (h_F) — beyond the generating plane (blade dedendum). The blade contours in Figure 3 are therefore not exactly congruent to each other, but by the backlash values different on the flanks and by the clearance values different at the roots (tips).

Since the aim in this first flank generating example is to achieve a conjugate pair, it seems appropriate to set the backlash SPLF for this example to zero.

As a result the following calculations will sufficiently determine the required cutter head and blade parameters:

$$t_B = \pi \times m_n = 12.57 \text{ mm} \tag{24}$$

$$SPLF = 0.00 \text{ mm} \tag{25}$$

Table 3 Cutter head and blade specifications			
Cutter Head and Blade Data			
Variable	Explanation	Value	Dimension
S8901,2	reference point to blade tip pinion	4.80	mm
S8903,4	reference point to blade tip gear	4.80	mm
WAME ₁	blade phase angle pinion convex	0.00	°
WAME ₂	blade phase angle pinion concave	0.00	°
WAME ₃	blade phase angle ring gear convex	0.00	°
WAME ₄	blade phase angle ring gear concave	0.00	°
XSME _{1,2}	blade offset in pinion cutter head	0.00	mm
XSME _{3,4}	blade offset in ring gear cutter head	0.00	mm
RCOW ₁	cutter point radius pinion inside blade	74.80	mm
RCOW ₂	cutter point radius pinion outside blade	77.59	mm
RCOW ₃	cutter point radius ring gear inside blade	81.09	mm
RCOW ₄	cutter point radius ring gear outside blade	71.31	mm
ALFW ₁	blade angle pinion inside blade	20.00	°
ALFW ₂	blade angle pinion outside blade	20.00	°
ALFW ₃	blade angle ring gear inside blade	20.00	°
ALFW ₄	blade angle ring gear outside blade	20.00	°

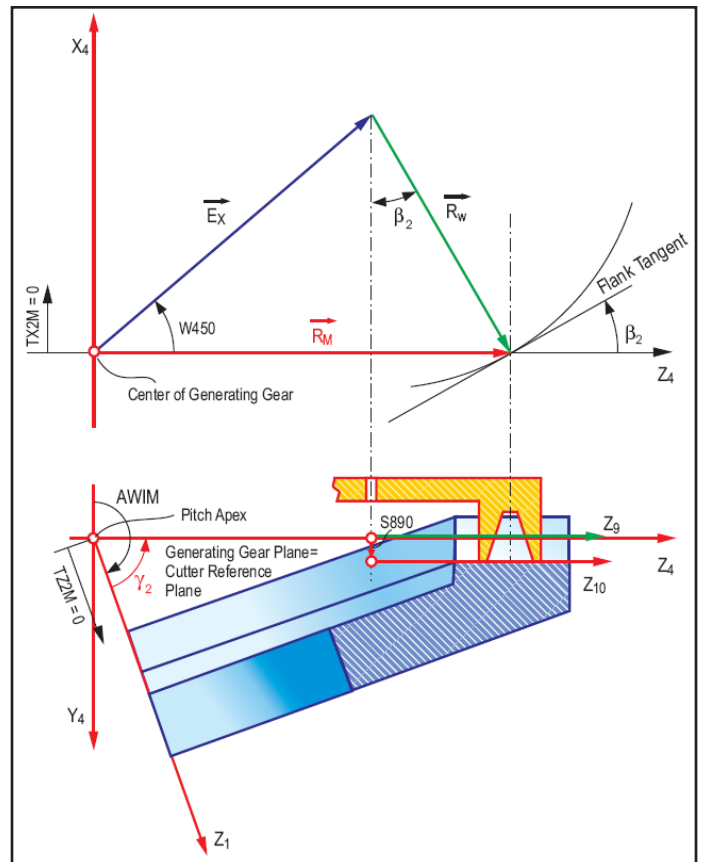


Figure 4 Ring gear, basic machine model: upper graphic — front view; lower graphic — top view.

$$ALFW_1 = ALFW_2 = ALFW_3 = ALFW_4 = \alpha = 20.00^\circ \quad (26)$$

$$RCOW_1 = R_W - t_B/4 - SPLF/4 - h_{F1} \times \tan ALFW_1 = 74.80 \text{ mm} \quad (27)$$

$$RCOW_2 = R_W + t_B/4 + SPLF/4 - h_{F1} \times \tan ALFW_2 = 77.59 \text{ mm} \quad (28)$$

$$RCOW_3 = R_W + t_B/4 - SPLF/4 + h_{F2} \times \tan ALFW_3 = 81.09 \text{ mm} \quad (29)$$

$$RCOW_4 = R_W - t_B/4 + SPLF/4 - h_{F2} \times \tan ALFW_4 = 71.31 \text{ mm} \quad (30)$$

$$S890_1 = S890_2 = h_{F1} = 4.80 \text{ mm} \quad (31)$$

$$S890_3 = S890_4 = h_{F2} = 4.80 \text{ mm} \quad (32)$$

All parameters printed in bold are required for the definition of the pinion and ring gear cutter heads required. Those results are summarized in Table 3.

Calculation of Basic Settings for the Cutting Machine

The basic machine, as defined by Weck and Schriefer (Ref. 3), follows a clear systematic with 10 coupled Cartesian coordinate systems, beginning with system 1, which defines the work gear position via system 4 which defines the generating gear plane with its axes X_4 - Z_4 and the generating gear axis with its axis Y_4 to system 10, which defines the cutter head axis with Y_{10} and the position of the blade origin (blade tip) with Z_{10} .

Figure 4 only includes the systems 1, 4, 9 and 10—which are required for the basic bevel gear calculation covered in this chapter.

The observations and machine setting calculation are first conducted for the ring gear and then the pinion. First we observe the generating gear plane X_4 - Z_4 (Fig. 4), in which the mean cone distance R_M is drawn from the origin of the coordinate system along the positive Z_4 axis. At the tip of the R_M vector, the mean face position is located, which is the point of a curved tooth, where the spiral angle β has to be equal 30° . The spiral direction shown in Figure 4 is consistent with a right-hand ring gear that has a mating pinion with a left-hand spiral direction (the view in Figure 4 is directed to the back-side of the ring gear). The spiral angle in each point of a flank is the angle in the generating gear plane between the flank tangent and the connecting line to the generating gear axis. In Figure 4 it is the angle β between flank tangent and Z_4 axis. This now allows the positioning of the cutter radius vector R_W with its tip perpendicular to the flank tangent. The solution vector in this observation is the eccentricity vector E_X , which already includes a number of machine settings.

$$\vec{E}_X = \vec{R}_M - \vec{R}_W \quad (33)$$

$$\text{With: } \vec{R}_M = \{0., 0., R_M\} = \{0., 0., 86.34\} \quad (34)$$

$$\vec{R}_W = R_W \{-\cos \beta, 0., \sin \beta\} \quad (35)$$

$$\vec{R}_W = \{-R_W \cos \beta, 0., R_W \sin \beta\} = \{-65.99, 0., 38.10\} \quad (36)$$

$$\text{Resulting in: } \vec{E}_X = \{65.99, 0., 48.24\} \quad (37)$$

Utilizing the E_X vector, the following machine settings can be calculated:

$$\text{Center roll position: } W450_{3,4} = \arctan(E_{XX}/E_{XZ}) = 53.83^\circ \quad (38)$$

$$\text{Radial distance: } TZMM_{3,4} = \sqrt{E_{XX}^2 + E_{XZ}^2} = 81.74 \text{ mm} \quad (39)$$

$$\text{Sliding base: } TYMM_{3,4} = E_{XY} = 0.00 \text{ mm} \quad (40)$$

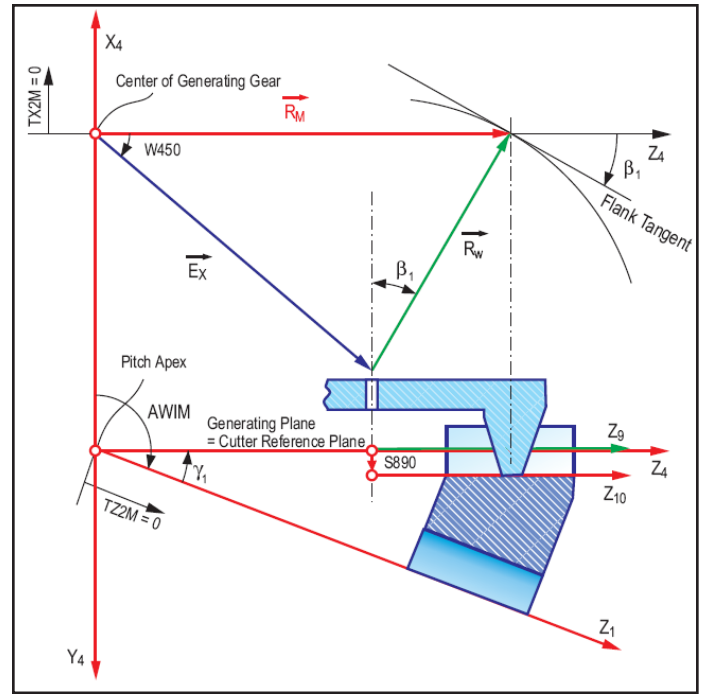


Figure 5 Pinion basic machine model: upper graphic—front view; lower graphic—top view.

Additional machine settings can be found from the graphical relationship in Figure 4:

$$\text{Machine root angle: } AWIM_{3,4} = -90^\circ - \gamma_2 = -159.62^\circ \quad (41)$$

$$\text{Machine center to crossing point: } TZ2M_{3,4} = 0.00 \text{ mm} \quad (42)$$

$$\text{Offset in the machine: } TX2M_{3,4} = 0.00 \text{ mm} \quad (43)$$

Further values such as cutter head tilt $WXMM_{3,4}$ and tilt orientation $WYMM_{3,4}$ are also zero in the observed conjugate design.

For the exact definition of the ring gear to be generated, the ratio of roll between generating gear and work gear is still missing. Using (Chapter 1, Part II, July *Gear Technology*) Equations 11 and 12, the ratio of roll can be computed with:

$$UDIF_{3,4} = \sin \gamma_2 = 0.937404 \quad (44)$$

The ratio of roll number requires at least a mantissa with 6 digits, since the influence onto the gear geometry is correspondingly sensitive.

The second part of the machine setting calculations, the demonstrated gear calculations are repeated analogous for the pinion. At first, we observe the generating gear plane X_4 - Z_4 (Fig. 5) in which the mean cone distance R_M is plotted from the coordinate origin along the positive Z_4 axis.

At the tip of the R_M vector, the mean face position of a curved tooth is located whose tangent in this point should show a spiral angle β of 30° . The spiral direction shown in Figure 5 is consistent with a left-hand pinion (in Fig. 5 (top) the view is directed from the back to the pinion). The spiral angle in each point of a flank is the angle in the generating gear plane between the flank tangent and the connecting line to the generating gear axis. In Figure 5 it is the angle β between flank tangent and Z_4 axis. This allows now the positioning of the cutter radius vector R_W with its tip perpendicular to the flank tangent. The solution vector

Table 4 Geometrical and kinematical machine settings

Machine Basic Settings			
Variable	Explanation	Value	Dimension
WXMM _{1,2}	cutter head tilt pinion	0.00	°
WXMM _{3,4}	cutter head tilt ring gear	0.00	°
WYMM _{1,2}	swivel angle pinion	0.00	°
WYMM _{3,4}	swivel angle ring gear	0.00	°
W450 _{1,2}	center of roll position pinion	-53.83	°
W450 _{3,4}	center of roll position ring rear	53.83	°
TYMM _{1,2}	sliding base position pinion	0.00	mm
TYMM _{3,4}	sliding base position ring gear	0.00	mm
TZMM _{1,2}	radial distance pinion	81.74	mm
TZMM _{3,4}	radial distance ring gear	81.74	mm
AWIM _{1,2}	machine root angle pinion	-110.38	°
AWIM _{3,4}	machine root angle ring gear	-159.62	°
TX2M _{1,2}	pinion offset in the machine	0.00	mm
TX2M _{3,4}	ring gear offset in the machine	0.00	mm
TZ2M _{1,2}	machine center to crossing point pinion	0.00	mm
TZ2M _{3,4}	machine center to crossing point gear	0.00	mm
UTEI _{1,2}	indexing ratio of pinion cutting	0.00	-
UTEI _{3,4}	indexing ratio of ring gear cutting	0.00	-
UDIF _{1,2}	ratio of roll for pinion cutting	0.348245	-
UDIF _{3,4}	ratio of roll for gear cutting	0.937404	-

in this observation is the eccentricity vector E_x , which already includes a number of machine settings.

$$\text{With: } \vec{R}_w = \{R_w \cos \beta, 0, R_w \sin \beta\} = \{65.99, 0, 38.10\} \quad (45)$$

$$\text{Resulting in: } \vec{E}_x = \{-65.99, 0, 48.24\} \quad (46)$$

By means of the E_x vector the following machine settings can be calculated:

$$\text{Center of roll: } W450_{1,2} = \arctan(E_{xx} / E_{xz}) = -53.83^\circ \quad (47)$$

$$\text{Radial distance: } TZMM_{1,2} = \sqrt{E_{xx}^2 + E_{xz}^2} = 81.74 \text{ mm} \quad (48)$$

$$\text{Sliding base: } TYMM_{1,2} = E_{xy} = 0.00 \text{ mm} \quad (49)$$

Additional machine settings can be found from the graphical relationship in Figure 5:

$$\text{Machine root angle: } AWIM_{1,2} = -90^\circ - \gamma_1 = -110.38^\circ \quad (50)$$

$$\text{Machine center to crossing point: } TZ2M_{1,2} = 0.00 \text{ mm} \quad (51)$$

$$\text{Offset in the machine: } TX2M_{1,2} = 0.00 \text{ mm} \quad (52)$$

Further values, such as cutter head tilt $XMM_{1,2}$ and tilt orientation $WYMM_{1,2}$ are also zero in the observed conjugate design.

For the exact definition of the pinion to be generated, the ratio of roll between generating gear and work gear is still missing. From (Chap. 1, Part II, July *Gear Technology*) Equations 11 and 12, the ratio of roll can be computed with:

$$UDIF_{1,2} = \sin \gamma_{12} = 0.348245 \quad (53)$$

All bold-printed values calculated in this section are input values for a bevel gear cutting simulation program, whose functionality is discussed in the next section. The machine settings are summarized in Table 4.

Simulation of the Gear Cutting Process and Tooth Contact Analysis of Face-Milled Spiral Bevel Gearset Example

A typical example of a simulation program is the FVA *Bevel-Gear-Chain*, which was developed at the Machine Tool Laboratory of the University of Aachen (Ref. 3). Some of today's commercially available software systems for bevel gear calculation and optimization have been developed on the basis of this universal software tool. The analysis and experimentation, introduced in the following chapters, are also based on an advanced version of the FVA *Bevel-Gear-Chain*. This software utilizes the same data as is used in modern free-form bevel gear cutting and grinding machines for the manufacture of real bevel gear sets. The core of this program is a flank generating module that applies the coordinate systems of Figures 4 and 5 to model a generating gear.

In the generating gear system $X_c - Y_c - Z_c$ (system S_c) in Figure 6, a generating gear flank point is given by position vector P_{csa} and normal vector N . The application of the gearing law (Chap. 1, Eq. 1, June *Gear Technology*) delivers the rotation angle φ_{ac} into the contact position (system S_a), in which the solution point P_c and the solution normal vector $-N$ is found in a coor-

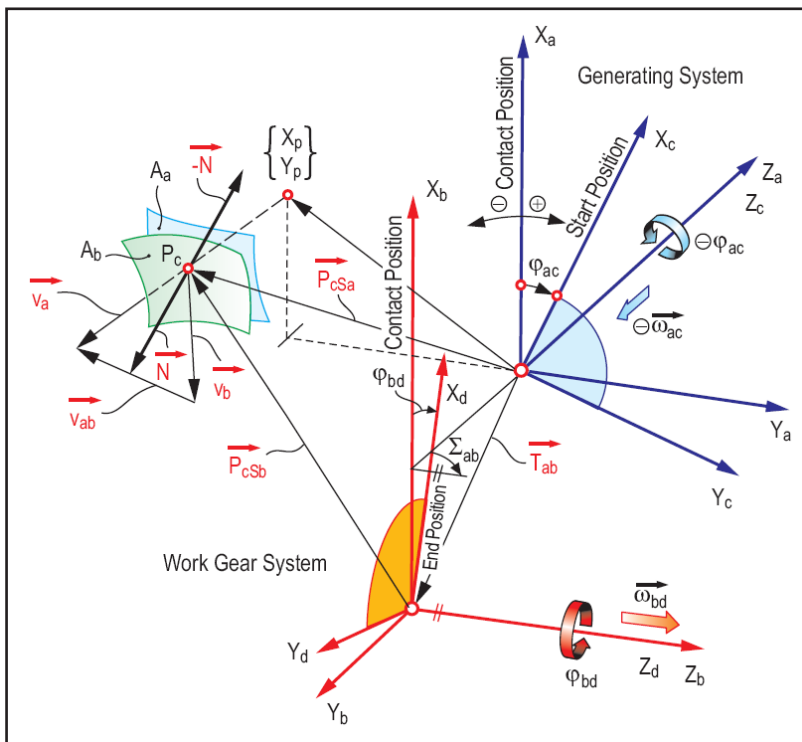


Figure 6 Kinematical relationships to solve gearing law equation.

ordinate system $X_b-Y_b-Z_b$ (system S_b) as position vector P_{csb} . In order to find a comprehensive flank as a result of computing a larger amount of individual points, which are necessary in order to define an entire flank (symbolized with surface A_b), the solution point has to be rotated “back” in its final position (system S_d). The angle φ_{bd} between the contact position and the final position is found by multiplication of the rotation angle φ_{ac} (in the generating gear system) with the ratio of roll. Figure 6 also shows that in the contact position the relative velocities $v_{ab} = v_a - v_b$ —and therefore the sliding and rolling velocities—can be determined rather easily.

The cutting edges, which are defined in the input data as lines, are treated in the flank surface generation program as a summation of discrete points; the rotation of the cutter head delivers a velocity vector in the respective cutting edge point. The vector product between the velocity vector and the cutting edge tangential vector results in a normal vector, which together with the cutting edge point, by solving the gearing law (as explained in Fig. 6), delivers a point and a normal vector of the work gear flank that is subject to the generating process. In a do loop the given number of cutting edge points — $YP10$ — are processed for each angular cutter head position (Fig. 7).

The result is the so-called “natural flank grid,” which ends at the root fillet but extends beyond the tooth boundaries in all other directions. It becomes evident from Figure 7 that the distortions of the natural flank grid are caused by the changing generating conditions. In order to achieve a flank grid—which fits the real tooth boundaries—the desired flank grid, known until now only in the $YRI-ZRI$ plane, is correlated to the natural grid (projected into the $YRI-ZRI$ plane). The distance of a respective point of the flank grid to the closest point of the natural grid leads to new given cutter head angle φ_{89Y} and cutting edge point $YP10$. The generating process with this new point will reduce the distance between the desired flank point and the actual generated point. This procedure is repeated in a semblance of an iteration until the distance lies within an iteration limit of usually 0.0002 mm. Flank surface points calculated with this method show an accuracy of 10^{-5} mm. The normal directions within the flank working area without undercut have deviations below half an angular minute.

The resulting flank surfaces are interpolated with bi-cubical spines in order to provide any in-between point with high accuracy during the following roll simulation between pinion and gear.

For the roll simulation the pinion flanks with their coordinate system $XRI-YRI-ZRI$ are located in the correct position relative to the ring gear flanks with their coordinate system $XRA-YRA-ZRA$. This relative position is defined by the shaft offset vector TT and the shaft angle Σ . The signified blanks of pinion and ring gear are shown in Figure 8. In the present example the shaft angle is 90° and the

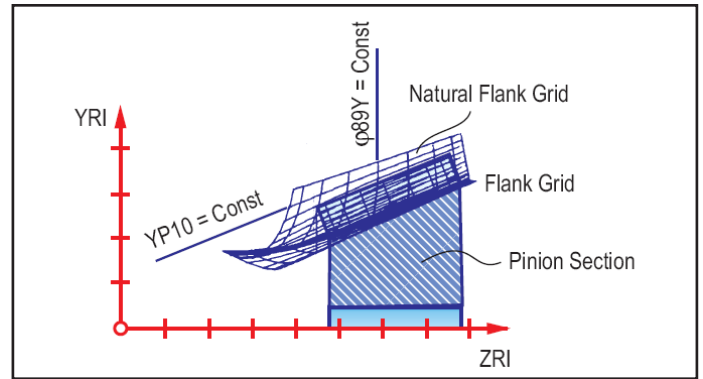


Figure 7 Flank grid and natural flank grid.

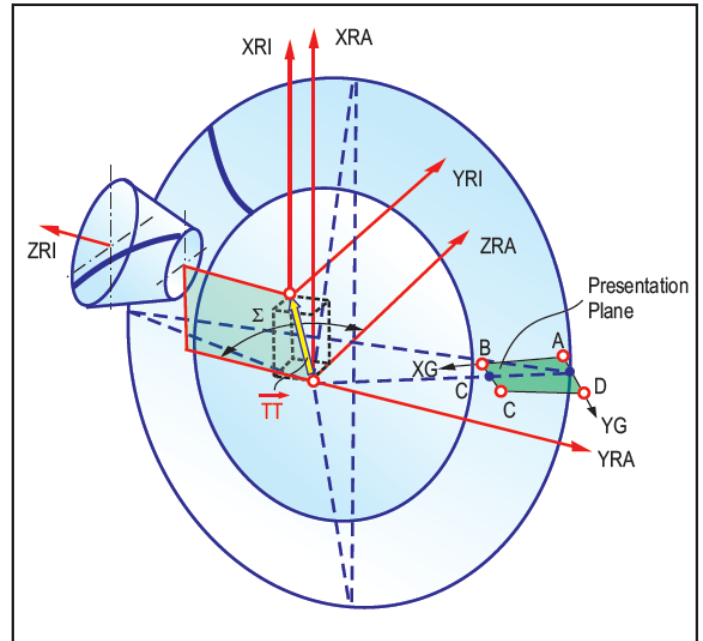


Figure 8 Arrangement of pinion and ring gear for roll simulation.

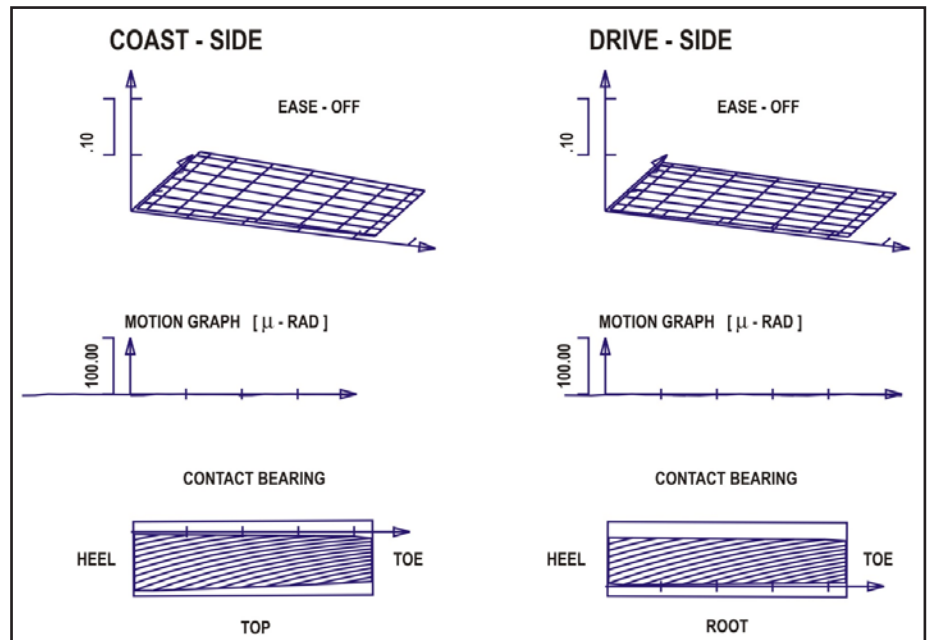


Figure 9 Graphical results of roll simulation (TCA) of face-milled gearset.

TT vector is zero — which defines a spiral bevel gearset without hypoid offset. In order to evaluate the properties of the gearset under load with deflected gear box housing, it is possible to use shaft angles that deviate from 90° together with any offset vector *TT*. The results of a roll simulation are Ease-Off, tooth contact pattern, and motion transmission error. In order to correlate those results in a meaningful way with the tooth flanks of the evaluated gearset, the flank projection into the plane *ZRA-YRA* (points *A, B, C* and *D*) is defined as presentation plane (Fig. 8). The Ease-Off is a three-dimensional graphic of the flank deviations from a conjugate pair; it is calculated by rolling the pinion flank “into” the gear coordinate system according to the gearing law, resulting in a virtual gear flank that is conjugate to the actual pinion flank. This conjugate gear flank will then be compared to the present gear flank, where all differences in arc length are plotted point-by-point in ordinate direction into the Ease-Off graphic.

If both mating bevel gears have conjugate manufacturing data, then the Ease-Off graphic has no deviations in ordinate direction. Also, if the pinion flanks and gear flanks have spiral angle errors of equal amounts, the Ease-Off graphic will not show any deviation. And although the individual gears are considered incorrect in this case, they will roll conjugate with each other, which subsequently leads to an Ease-Off without any ordinate values. Further explanations regarding roll simulation and tooth contact analysis results are presented in Chapter 4 (*Nov.-Dec. Gear Technology*).

The roll simulation analyses results of the bevel gearset calculated in this chapter (in its theoretical zero position) can be observed in Figure 9. In the left column the results of the coast-side are shown, which is the combination of the convex pinion flank and the concave ring gear flank. In the right column the results of the drive-side are shown, which is the combination of the concave pinion flanks and the convex ring rear flanks. The drive-side is the preferred flank combination; the reasons for the superior rolling conditions of the drive-side are discussed in Chapter 4.

Just like the theoretical goal, a conjugate gear pair with zero Ease-Off was created. The motion graphs in the middle section of Figure 9 only show some “numerical noise” along the abscissa of the diagrams, meaning there is no transmission error in any of the roll positions. The contact bearings in the lower section of Figure 9 show contact lines, which extend inside the entire flank working areas.

The flank working area is the common surface between the active pinion flank that is rolled with the active ring gear flank. For a better understanding of the flank working area, the previously mentioned rolling of the pinion flank into the ring gears coordinate system can be employed. If the resulting conjugate ring gear flank is projected into the presentation plane (rotational projection) where it overlays the area of the actual ring gear flank (which is already projected into the presentation plane), then the working area is defined as the area where both the conjugate gear flank and the real gear flank exist. It seems obvious that no flank contact or correct rolling outside of this area is possible. On the heel and toe borders only “air” is present outside of the working area of one of the two flanks (or both). At top and root either the rolled on top edge of the one flank, or

the border to the root fillet of the other flank is the limitation. Caution is required if the root fillet border is the limitation. In many cases this leads to interferences that can cause noise and surface damage. The flank working areas in Figure 9 end along the horizontal coordinate axis (coast-side on the top, drive-side on the bottom) that represent the transition line between flank and ring gear root fillet.

On the opposite sides (coast-side on the bottom, drive-side on the top) exists a non-working area between ring gear face edge and tooth contact zone, pointing to a “pulled-up” pinion root transition that migrates into undercut in the toe region. A pulled-up pinion root transition is more dangerous than undercut, since interferences can occur that can lead to flank surface damage, as mentioned above. The result in many cases is the population of pitting and even tooth fracture. Intentionally, no profile shift was applied in the present example in order to demonstrate the motivation to introduce a profile shift. In a simplified observation a negative ring gear profile shift with a magnitude equal to the white zone at the top of the ring gear tooth is required (app. 1.75 mm).


Profile shift:

$$\Delta h = x_2 \times m_n = x_2 \times 4.00 \text{ mm} = -1.75 \text{ mm} \tag{54}$$

$$x_2 = -0.448 \tag{55}$$

In bevel and hypoid gears, generally the *V0* system is applied, which allows determination of the pinion profile shift as:

$$V0 \equiv x_1 + x_2 = 0.00 \rightarrow x_1 = -x_2 = 0.448 \tag{56}$$

This will shorten the gear addendum and lengthen the gear dedendum, which will result in a match between the common flank area and the active flank working area. The region with incorrect roll conditions along the pinion root will be eliminated by using the optimal part of the involute. The white region along the ring gear top will now be filled with contact lines and the active flank working area will be maximized. 

Dr. Hermann J. Stadtfeld received in 1978 his B.S. and in 1982 his M.S. degrees in mechanical engineering at the Technical University in Aachen, Germany; upon receiving his Doctorate, he remained as a research scientist at the University’s Machine Tool Laboratory. In 1987, he accepted the position of head of engineering and R&D of the Bevel Gear Machine Tool Division of Oerlikon Buehrle AG in Zurich and, in 1992, returned to academia as visiting professor at the Rochester Institute of Technology. Dr. Stadtfeld returned to the commercial workplace in 1994 — joining The Gleason Works — also in Rochester — first as director of R&D, and, in 1996, as vice president R&D. During a three-year hiatus (2002–2005) from Gleason, he established a gear research company in Germany while simultaneously accepting a professorship to teach gear technology courses at the University of Ilmenau. Stadtfeld subsequently returned to the Gleason Corporation in 2005, where he currently holds the position of vice president, bevel gear technology and R&D. A prolific author (and frequent contributor to *Gear Technology*), Dr. Stadtfeld has published more than 200 technical papers and 10 books on bevel gear technology; he also controls more than 50 international patents on gear design, gear process, tools and machinery.

